Magnetic and collisional effects on presheaths

G.-H. Kim,[a] N. Hershkowitz,[b] D. A. Diebold, and M.-H. Cho[c]
Department of Nuclear Engineering and Engineering Physics, University of Wisconsin—Madison, 1500 Johnson Drive, Madison, Wisconsin 53706

(Received 13 February 1995; accepted 17 March 1995)

The effects of both magnetic field and collisions on presheath properties are experimentally investigated in plasmas with electron temperatures much greater than ion temperatures. Measurements of plasma potential in collisionless plasmas show presheath thicknesses at boundaries oblique to magnetic field to be approximately $(C_s/\omega_{ci})\sin\psi$, where C_s is the ion sound speed, ω_{ci} is the ion gyrofrequency, and Ψ is the angle between the magnetic field and the normal to the wall boundary. Measurements of plasma potential in collisional plasmas find presheaths consisting of two distinctive regions. With ion–neutral collision mean-free path $\lambda_n < (C_s/\omega_{ci})\sin\psi$, the presheath region next to the sheath has collisional characteristics and a thickness of approximately $(0.5-0.6)\lambda_n$. The corresponding presheath region adjacent to the bulk plasma has magnetic characteristics and a thickness of approximately $(0.5-0.9)(C_s/\omega_{ci})\sin\psi$. Equipotential contours in the collisional region of this presheath are found to be parallel to the boundary, while those in the magnetic region are not. © *1995 American Institute of Physics.*

I. INTRODUCTION

It has been known for some time[1] that sheaths form between plasmas and objects in contact with them. When the potential difference Φ between a collisionless, unmagnetized plasma and an object is smaller than the electron temperature T_e, then the sheath dimension λ_s is approximately the Debye length λ_D. For $e\Phi > T_e$, $\lambda_s \approx \lambda_D (e\Phi/T_e)^{3/4}$.

In practice, [e.g., wafer etching in electron cyclotron resonance (ECR) devices,[2] erosion of and power transfer to (gaseous) divertors and limiters in fusion devices,[3] double layers in space plasmas,[4] and Langmuir probe operation[5]], λ_s is usually much smaller than the corresponding collisional and magnetic scale lengths; and, hence, collisional and magnetic field effects on sheaths are often not serious. Presheaths, however, have much larger dimensions than sheaths, and can, in general, be significantly influenced by collisional and magnetic effects.

Presheaths form between sheaths and plasmas when $T_i < T_e$. The Bohm sheath criterion[6–10] states that ions entering a collisionless, unmagnetized sheath must have an average directed velocity $\langle V_B \rangle$ *normal*[7,8] to the sheath edge of at least the ion sound velocity C_s (for this paper, we assume $C_s = \sqrt{T_e/m_i}$ since $T_i \ll T_e$, where m_i is the ion mass), i.e., $\langle V_B \rangle \geq C_s$. When $T_i < T_e$, there is a presheath[10] between the plasma and the sheath that accelerates ions, so that the Bohm criterion[6–10] is met. For the special case of unmagnetized, collisionless plasmas with $T_i \ll T_e$, the presheath dimension[11,12] λ_{ps} is approximately half the plasma dimension $L/2$, and the potential difference[10] Φ_{ps} across the presheath is greater than or equal to $T_e/2e$. Note that although there has been some theoretical justification[11,13] for presheaths in unmagnetized, collisionless plasmas when $T_i \geq T_e$, there have been no experimental data suggesting such presheaths.

The emphasis of this paper is magnetic and collisional effects on presheaths. Although there has been substantial theoretical work on collisional effects[14,15] and, to a lesser extent, on magnetic effects on presheaths,[16–19] there has been, to our knowledge, only one direct measurement of collisional effects on presheaths[2] and no direct measurements of magnetic effects on presheaths. Furthermore, models[20,21] that address simultaneous collisional and magnetic field effects on presheaths (they are discussed in detail in the next section) are in a preliminary stage.

Here we present plasma potential data showing, for the first time, magnetic effects on presheaths in both collisionless and collisional low temperature ($T_i \ll T_e$) plasmas with $\lambda_s \ll r_{cs} \ll L/2 \leq \lambda_n$ and $\lambda_s \ll \lambda_n \leq r_{cs} \ll L/2$, respectively, where r_{cs} is the ion sound gyroradius, $r_{cs} \equiv C_s/\omega_{ci}$, and λ_n is the ion–neutral collision mean-free path, which is the dominant collision mean-free path in this study. This paper is organized as follows: In Sec. II, previous studies, especially theoretical studies, are reviewed. In Sec. III, the experimental apparatus and technique are described. In Secs. IV and V, discussions of magnetic presheath and magnetic-collisional presheath, respectively, experimental results and comparisons with available theories are presented. Conclusions are presented in Sec. VI.

II. THEORETICAL BACKGROUND

Figure 1 is a schematic of the situation considered in this paper. The bulk plasma has $T_i \ll T_e$. Like most practical cases, the sheath shown is unmagnetized and collisionless because λ_s is much less than r_{cs} and λ_n. Note that the Bohm sheath criterion applies to unmagnetized, collisionless sheaths and, hence, also to the situation depicted in Fig. 1. The criterion, which requires an average velocity $\langle V_B \rangle$

[a]Present address: Department of Physics, Hanyang University, Ansan-si, Kyungki-do, 425-791, South Korea.
[b]Also affiliated with the Engineering Research Center for Plasma-Aided Manufacturing, University of Wisconsin—Madison, 1410 Johnson Drive, Madison, Wisconsin 53706.
[c]Present address: Department of Physics, Pohang Institute of Science and Technology, P.O. Box 125, 790-330, South Korea.

 1070-664X/95/2(8)/3222/12/$6.00

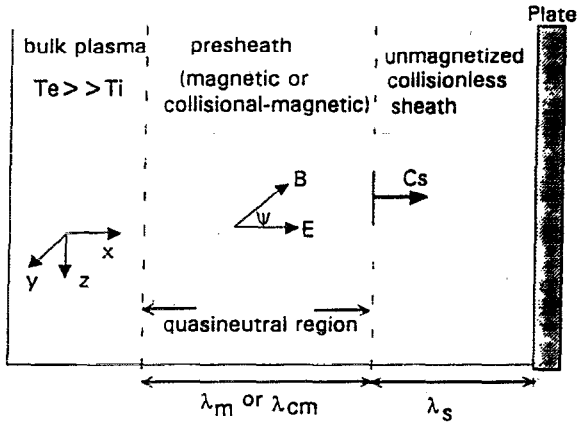

FIG. 1. Schematic of the sheath and the presheath considered. When the magnetic field is applied to the collisionless plasma, the presheath (with thickness λ_p) becomes the magnetized presheath (with thickness $\lambda_p=\lambda_m$); when the plasma is collisional, the presheath becomes the collisional presheath (with $\lambda_p=\lambda_c$); and when an oblique magnetic field is applied to a collisional plasma, presheath becomes the collisional-magnetic presheath (with $\lambda_p=\lambda_{cm}$). Ions that enter the sheath must do so with a minimum velocity of C_s normal to the sheath/presheath boundary.

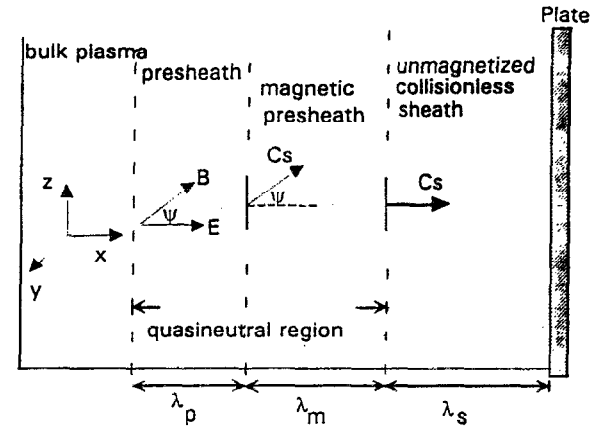

FIG. 2. Schematic of Chodura's presheath model.[7] The ion velocity entering the magnetic presheath is C_s along the magnetic field, and the ion velocity entering the sheath (λ_s) is C_s normal to the sheath boundary. Here λ_p is an additional presheath thickness.

normal[7–9] to the sheath edge of at least C_s, is represented in Fig. 1 as the arrow labeled C_s at the sheath/presheath boundary.

All presheaths considered in this paper are magnetized. In the absence of collisions, presheaths and the thickness of presheaths will be referred to as magnetic presheaths and λ_m, respectively. The corresponding terminology in the presence of collisions will be collisional-magnetic presheaths and λ_{cm}.

A. Magnetic presheaths

Most studies of sheaths and presheaths have investigated collisionless, unmagnetized plasmas (see Ref. 14 for further literature); only a few have addressed magnetic field effects.[16–19] For $\Psi=90°$, where Ψ is the angle between the magnetic field and the normal to the wall boundary, Theihaber *et al.*[22] showed through particle simulations that the cross-field sheath was a highly turbulent region caused by the Kelvin–Helmholtz instability. Daybelge and Bein[18] considered magnetic field effects on sheaths when $\Psi\cong 90°$, and concluded that the sheath potential Φ_s was independent of Ψ. Unfortunately, Daybelge and Bein did not consider presheaths. Hence, their work is not applicable to the experimental work presented here for which $T_i \ll T_e$ and, therefore, presheaths are present. DeWald *et al.*[19] considered magnetic effects when $0°<\Psi<90°$; and, like Daybelge and Bein, they found that Φ_s was independent of Ψ.

Of the theoretical works to date, the work by Chodura[16] is perhaps the most applicable to the experiments described here. Chodura considered magnetic field effects for $0°<\Psi<90°$. However, unlike Deybelge and Bein, he included presheaths; and unlike DeWald *et al.*, he required that ions entering the sheath satisfy $\langle V_B\rangle \geq C_s$, the generalized Bohm sheath criterion for unmagnetized, collisionless sheaths. One may wish to note, if reading Chodura, that he did not refer the criterion $\langle V_B\rangle \geq C_s$ as the generalized Bohm sheath criterion for unmagnetized, collisionless sheaths, but rather as "it is arbitrary and is justified afterward from the results."[16]

The sheaths and presheaths that Chodura's simulations considered are depicted in Fig. 2. A comparison of Figs. 1 and 2 shows that the region that we (Fig. 1) refer to as the magnetic presheath is, in Chodura's model (Fig. 2), not one region but two regions: the presheath and the magnetic presheath. In addition to the Bohm sheath criterion (which is represented in Fig. 2 as $V_s=C_s$ at the sheath/magnetic presheath boundary), Chodura assumed (for achieving a stable numerical solution) that the ions enter the magnetic presheath with an average velocity $\langle V_\parallel\rangle$ *along* the magnetic field line greater than or equal to C_s. This is shown in Fig. 2 as the arrow labeled C_s that is parallel to B (i.e., $V_{x0}=C_s\cos\Psi$) at the presheath/magnetic presheath boundary. He referred to this assumption that $\langle V_\parallel\rangle \geq C_s$ as the generalized Bohm condition for an oblique magnetic field [see Eq. (12) in Ref. 16]. However, the necessity of this condition is questionable.[14,19] Furthermore, there is the question of the appropriate nomenclature to be used in describing the region, the magnetic presheath, between the presheath and the electrostatic Debye sheath in this paper, because the ions entering into the magnetic presheath satisfy this special Bohm criterion for the magnetic field while the magnetic presheath plasmas satisfy the quasineutrality condition [see Eq. (11) in Ref. 16].

Chodura[16] numerically found a magnetic presheath thickness,

$$\lambda_m^T=\sqrt{6}r_{cs}\sin\psi, \tag{1}$$

and a potential drop across the magnetic presheath,

$$\Phi_m^T=-\frac{T_e}{e}\ln\left(\frac{V_{xs}}{V_{x0}}\right), \tag{2}$$

where V_{x0} and V_{xs} are the ion velocities in the direction normal to the object boundary of ions entering and exiting the magnetic presheath region, respectively. Using his magnetic presheath boundary conditions $V_{x0}=C_s\cos\psi$ and $V_{xs}=C_s$, Eq. (2) can be rewritten as

$$\Phi_m^T = \frac{T_e}{e} \ln(\cos \psi). \quad (3)$$

Chodura also found that the total potential drop Φ across the sheath and presheath in front of the target, for constant bulk plasma density and constant flow velocity conditions, is insensitive to Ψ. The reader may wish to note that when Φ is constant (as Chodura found), increasing Ψ increases the potential drop Φ_m across the magnetic presheath and, consequently, the potential drop Φ_s across the Debye sheath decreases.[23]

B. Collisional-magnetic presheaths

In ECR[2] and gaseous divertor plasmas,[24] particle behavior in presheaths may be affected by the collision mean-free path as well as by the oblique magnetic field ($0°<\Psi<90°$). Most theoretical studies of collisional effects on sheaths and presheaths have been carried out for unmagnetized plasmas (see Ref. 14 for more information). Behnel[21] attempted to solve the ion-Boltzmann distribution for a given potential in a collisional plasma with $\Psi=90°$, but he did not obtain a self-consistent solution.

Riemann[20] has calculated the presheath potential Φ_{ps} dependence on the ratio α of the collision frequency to the ion gyrofrequency, and found that with decreasing collision frequency for $\alpha \gg 1$, Φ_{ps} increases due to the decreasing transport coefficient perpendicular to the magnetic field. As $\alpha \rightarrow 1$, the transport parallel to the magnetic field becomes dominant. With a further decrease of the collision frequency, Φ_{ps} decreases due to the enhancement of the parallel transport coefficient. The extreme case of no collisions is that which Chodura considered. In the absence of collisions, Riemann claimed that the region $\langle V_\parallel \rangle \geq C_s$ is not distinguished by the onset of the magnetic field effects as Chodura claimed, but rather by the transition from mobility to inertia controlled motion.

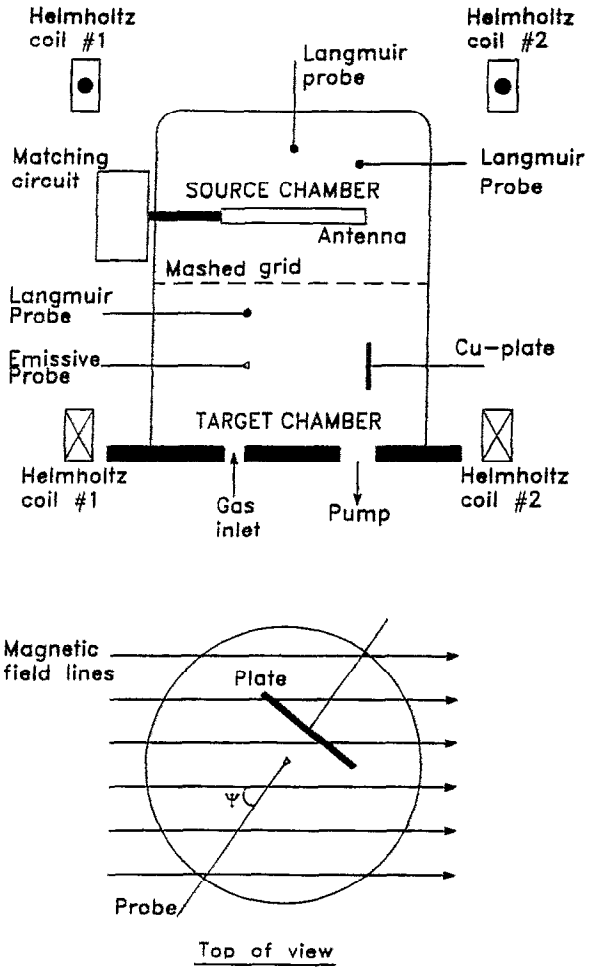

FIG. 3. Schematic illustration of the modified ISD chamber (top) and the geometry of the model cell in the target chamber showing the magnetic field lines with the grounded target plate (bottom).

III. EXPERIMENTAL APPARATUS AND TECHNIQUES

A. Inductive source device ISD

Measurements of collisionless, magnetic presheaths were carried out in an inductive source device ISD; see Fig. 3. Up to 500 W of RF power (13.56 MHz) was delivered to a resonant tank circuit, which consisted of a single turn loop antenna and external capacitors. The antenna (a dielectric coated copper strip of 4.3 cm width and 18 cm diam) was located at the center of a thin wall (0.92 mm) stainless steel chamber (35 cm diam, 40 cm length), and 28 cm from the bottom of the chamber. In order to reduce RF noise, the target chamber was separated from the source chamber by a grounded stainless steel mesh grid (0.5 mm×0.5 mm) which was located 22 cm from the bottom of the chamber. Uniform DC magnetic fields ranging from 40 to 170 G were applied to the target plasma by external Helmholtz coils. The upper limit of 170 G was set by the maximum magnetic field strength available. For $B<30$ G, it was observed that the plasma was dense but unstable, because the electron cyclotron resonance was too close to the RF frequency. The orientation of magnetic field with respect to the grounded target plate was adjusted by rotating the chamber (to which the plate was attached). In the target chamber of ISD, the bulk plasma potential was fairly uniform in the central region (approximately 25 cm), with the exception of the plasma potential along the field lines that mapped to the grounded screen protecting the vacuum pump. To reduce chamber wall sheath effects, the copper target plate (15 cm in diameter) was located 8 cm from the wall.

Helium was chosen as the working gas because helium plasmas are relatively high-temperature plasmas, as compared to argon or nitrogen plasmas of similar plasma densities. This allowed for longer Debye lengths and sheath thickness. Under a constant neutral gas pressure and input power, it was observed that T_e was insensitive to B. Vents to air were required to rotate the chamber to change the angle Ψ. These vents were found to have little effect on plasma performance.

To minimize collisional effects, the experiments were carried out in low-pressure plasmas. Typical plasma parameters in ISD were neutral pressure $P_0 \sim 0.1-0.5$ mTorr, $n_e \sim 5\times10^7$ cm^{-3}, $T_e \sim 6-8$ eV (7.1 ± 0.4 eV from the mea-

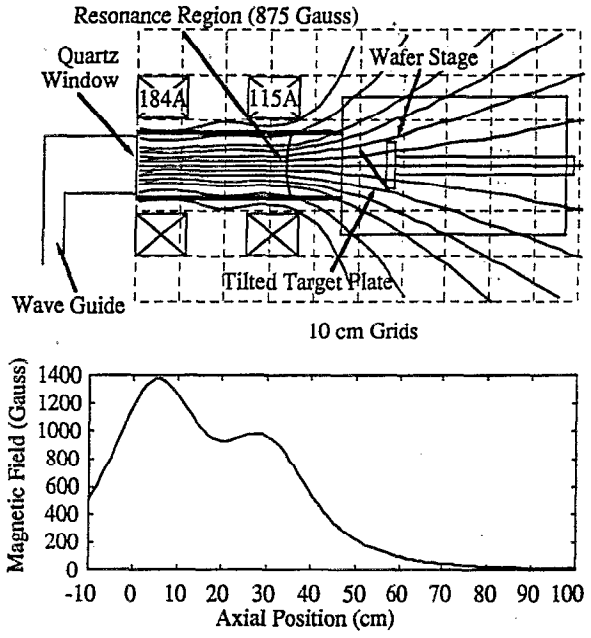

FIG. 4. Schematic illustration of the ECR etching device showing the magnetic field lines and resonance zones (top) and the magnitude of the axial magnetic field (bottom).

surement of ion acoustic speed), and $T_i<0.3$ eV (from ion energy analyzer measurements). The mean-free path for helium ion neutral collisions and charge exchange collisions[25] were approximately the diameter of the chamber at $P_0\sim0.5$ mTorr. Hence, the plasma was collisionless. A typical Debye length λ_D for these plasmas was approximately 0.3–0.4 cm. While T_e and n_e were insensitive to P_0 and B in ISD, it was observed that the bulk plasma potential and floating potential increased for increasing the magnetic field. The potential drop Φ between the bulk plasma and the object was found to be approximately $\Phi\sim(T_e/e)(2.2+\ln B)$.[26]

B. Electron cyclotron resonance (ECR) etching device

An electron cyclotron resonance (ECR) etching device (see Fig. 4) was used to study collisional-magnetic presheaths. This device has been described elsewhere,[2] and will only briefly be described here. In this device, microwave power $\leqslant$1000 W at 2.45 GHz (from an ASTeX S1000 source) can be coupled to the plasma through a quartz window at the end of the source chamber. Plasma is resonantly produced in the mirror cell of the source chamber and allowed to flow out along an expanding magnetic field into the downstream (or target) chamber. The magnetic fields encountered a titled, grounded tantalum plate (11 cm diam) on a wafer stage that was located 10 cm from the source chamber. The grounded plate was rotated up to 40° with respect to the wafer stage, which was the maximum available angle in this system. The magnetic field decreased from about 200 to 150 G (near the plate) in the scanning region. In our experiment, the magnetic field strength is assumed to be 175 G. Also, the field lines were slightly divergent; the divergence

TABLE I. Experimental plasma parameters of ISD and ECR devices.

System	ISD	ECR
RF (MHz)	13.56	2450
Gas (amu)	He (4)	N_2 (28)
P_0 (mTorr)	0.1–0.5	0.75–2
power (W)	200	800
B (G)	30–170	150–200
Ψ (°)	30–80	0–40
n_e (cm^{-3})	$\sim5\times10^7$	$\sim10^{10}$
T_e (eV)	6–8	3–5
T_i (eV)	<0.3	<0.3
λ_n (cm)	>50	$\leqslant$5
λ_{De} (cm)	~0.3	~0.01
$r_{cs}=C_s/\omega_{ci}$ (cm)	~3 (@170 G)	~5.3 (@175 G)

was less than 5° between the center and the edge of the plate. Therefore, there may be some small error caused by the magnetic field nonuniformity.

The measurements in the ECR device were performed in nitrogen plasmas with 800 W of microwave power and neutral pressures of 0.75 and 2 mTorr with constant nitrogen flow rates of 7.2 sccm and 22.7 sccm, respectively. It was found that the bulk plasma potential did not vary with plate rotation. The ion–neutral collision mean-free paths λ_n were approximately 3.5 and 1 cm at these pressures.[2] These λ_n were less than both the system dimension and the size of target plate, but they were comparable to r_{cs}. Hence, presheaths were collisional and magnetized. Typical plasma parameters along the central axis were $n_e\sim10^{10}$ cm^{-3} and $T_e\cong3$ and 5 eV at the operating pressures of 2 and 0.75 mTorr, respectively. Electron temperatures near the source region in the ECR device were about 30% higher than in the target plate region; $T_e\sim4.75$ eV at 0.75 mTorr and 3.75 eV at 2 mTorr near the source chamber ($B\sim200$ G), while $T_e\sim3.75$ eV (0.75 mTorr) and 2.85 eV (2 mTorr) near the target plate region ($B\sim150$ G). Due to plasma ambipolar diffusion from the source, n_e near the source chamber was 10% higher than that near the target chamber. The ambipolar electric field was nearly constant with a value of 0.25 V/m, and had little pressure dependence.[10] The details of the parameters of ISD and ECR plasmas are summarized in Table I.

C. Diagnostics

Considerable care was taken to ensure accurate measurements from the diagnostic (Langmuir and emissive) probes that were used. Electron depletion along magnetic field lines[27] and electrostatic ion cyclotron noise[28] are both examples of phenomena generated by Langmuir probes in magnetic fields that can cause difficulty in obtaining accurate Langmuir probe measurements of n_e, T_e, and plasma potential Φ_p.

Langmuir probes were not employed in presheaths and sheaths, where even in the absence of magnetic field they can be inaccurate,[29] but were used to measure bulk plasma n_e and T_e in both the ISD and ECR devices. As a check, bulk T_e was also determined from ion acoustic speed measurements.[26]

Emissive probes were used to make plasma potential Φ_p measurements everywhere (i.e., in the sheath, presheath, and bulk plasmas) in both the ISD and ECR devices; and for each condition and at each position, Φ_p was measured three times, and the measurements were then averaged. The most commonly used and convenient emissive probe technique, the floating point of a strongly emitting probe technique,[30] does not always work well in sheaths,[31] and was not used here. Rather, the inflection point in the limit of the zero emission technique[32] was employed.

Smith *et al.*[32] demonstrated that in the limit of zero emission the inflection point of the current-voltage characteristic of an emitting probe is a good measure of Φ_p in magnetized plasmas, as well as field-free plasmas. Other advantages of this technique are the following: it works well in sheaths and presheaths, it is not sensitive to the presence of electron or ion beams, it does not require strong emission,[33] and it has an accuracy as good as 0.2 V (which is limited by the emitting wire temperature of 0.2 eV).[34] The reader may wish to note that along with this technique's many advantages, there are a few disadvantages, specifically it requires considerable care in finding the inflection point in the limit of zero emitting current and it is quite time consuming because Φ_p profiles must be measured point by point. The emissive probe consisted of a 2% thoriated tungsten wire (with a 2.54×10^{-3} cm diam and approximately 0.5 cm length), which was heated to thermionic emission by a DC power supply. The probe bias voltage was measured across a voltage divider to indicate the value at the middle of the wire. Measurements were taken every 0.5 cm in the normal direction to the plate. Positions were resolved to 0.1 cm by using a mechanical probe driver.

IV. MAGNETIC PRESHEATH EXPERIMENTAL RESULTS AND DISCUSSION

A. Magnetic presheath measurements in ISD

Figure 5(a) shows plasma potential Φ_p versus position data. The data were taken on the center axis of a grounded plate and Ψ (as shown in Fig. 3) was 60°. One spatial scan was made for each of the following magnetic fields: 43, 60, 85, and 170 G. As mentioned in the Experimental Apparatus and Techniques section, the variation in bulk Φ_p with B is an artifact of the plasma source operation, and is not due to sheath/presheath dynamics. In particular, the measured bulk Φ_p, and hence Φ (potential drop from bulk plasma to wall), did not vary as Ψ was varied, even though both the sheath Φ_s and the magnetic presheath Φ_m potentials varied.

To determine the positions of the sheath/magnetic presheath and the magnetic presheath/bulk plasma boundaries, the potential profiles were graphed on semilog and log–log plots. For example, Fig. 5(b) shows the semilog plot of 60 G data shown in Fig. 5(a). Note that there is a relatively flat slope in the bulk Φ_p (i.e., the bulk Φ_p is fairly uniform), a steeper slope in the magnetic presheath, and the steepest slope in the sheath region (where electric fields are the strongest). The positions of the boundaries are taken to be the positions where these slopes change. The sheath/magnetic presheath boundaries are denoted with upward arrows, while the magnetic presheath/bulk plasma boundaries are denoted with downward arrows. The distances between the upward and the downward arrows are the magnetic presheath thicknesses λ_m. Note that Fig. 5(a) clearly shows that the λ_m's increase with decreasing magnetic field. Also note that the magnetic presheaths have a region where the potential decreases linearly (i.e., a quasineutral region of nonzero constant electric field) and a transition region, where the potential decreases sharply (due to the start of the charge separation) to smoothly match the sheath. The data of Fig. 5(a) which show that λ_m (specifically, the constant electric field region) approaches the half of the chamber size with

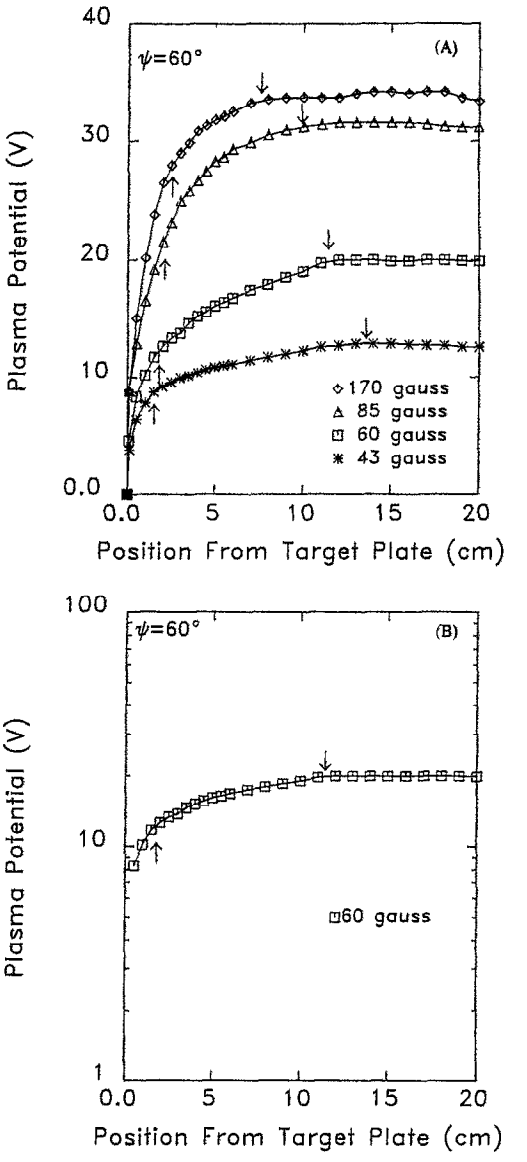

FIG. 5. (A) The plasma potential versus position from the ground plate at $\Psi=60°$ in an ISD helium plasma. The upward arrows indicate the sheath/magnetic presheath boundaries and the downward arrows indicate the presheath/bulk plasma boundaries. (B) Typical semilog plot of plasma potential (at 60 G, $\Psi=60°$) to define the magnetic presheath boundary. The upward arrow indicates the sheath/magnetic presheath boundary and the downward arrow indicates the magnetic presheath/bulk plasma boundary.

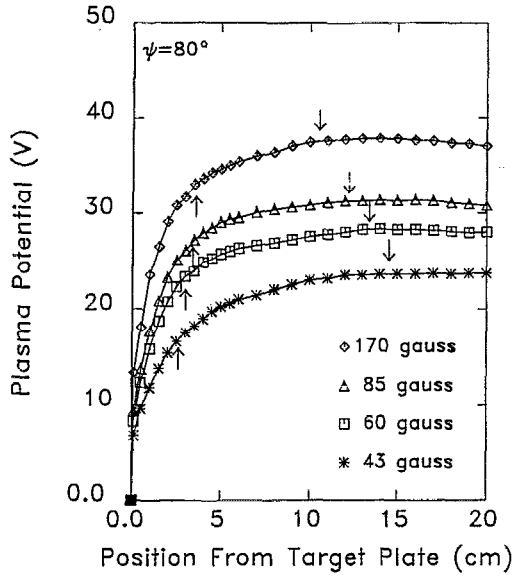

FIG. 6. The plasma potential versus position from the ground plate at $\Psi=80°$ in an ISD helium plasma. The upward arrows indicate the sheath/magnetic boundaries and the downward arrows indicate the magnetic presheath/bulk plasma boundaries.

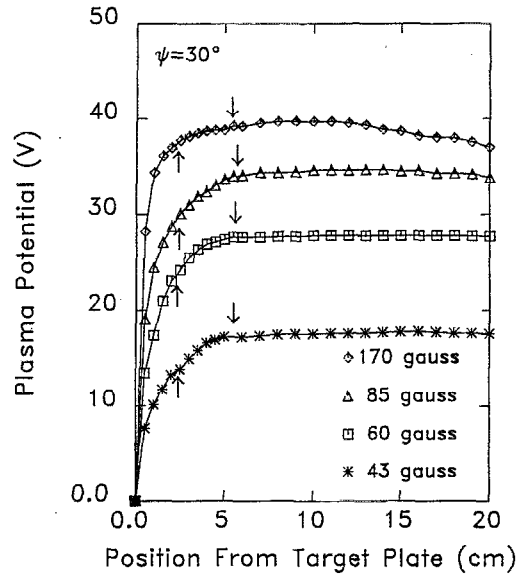

FIG. 7. The plasma potential versus position from the ground plate at $\Psi=30°$ in an ISD helium plasma. The upward arrows indicate the sheath/magnetic boundaries and the downward arrows indicate the magnetic presheath/bulk plasma boundaries.

decreasing B, suggest that the magnetic presheaths tend to become unmagnetized with decreasing B.

Figure 6 shows data taken at $\Psi=80°$. Similar to the data of Fig. 5, the data of Fig. 6 also show the λ_m's increase with decreasing B. Compared to the data at $\Psi=60°$, the λ_m's are larger. Thus, the combined data of Figs. 5 and 6 show that the magnetic presheath thickness λ_m depends on both B and Ψ. The bulk plasma potentials of Fig. 6 are slightly greater than those of Fig. 5. There was a vent to air between the time that the data of Figs. 5 and 6 were taken, the purpose of the vent, as mentioned in Sec. II, being to rotate the chamber to change Ψ. The differences between the bulk Φ_p shown in Figs. 5 and 6 are due to the slightly different plasma conditions, and not to the angle variations.

The data of Fig. 7, taken at $\Psi=30°$, show that λ_m's are insensitive to B at low field strengths. In particular, for $B\leqslant 85$ G, λ_m's are approximately constant. This behavior is due to finite boundary effects and is quantitatively analyzed in Sec. V C.

B. Experimentally determined thicknesses λ_m of magnetic presheaths

The data of Fig. 8 show that the measured thicknesses λ_m's of magnetic presheaths are described well by

$$\lambda_m \cong r_{cs} \sin\psi = (C_s/\omega_{ci})\sin\psi, \tag{4}$$

where r_{cs} is the ion sound gyroradius, Ψ is the angle between the magnetic field and the normal to the boundary, C_s is the ion acoustic sound speed, and ω_{ci} is the ion cyclotron frequency. Note that Fig. 8 includes the width associated with the magnetic region of collisional-magnetic presheaths (the N_2, ECR data). These data will be discussed in detail in Sec. V. Note for now that the magnetic region of presheaths is well described by Eq. (4), both in the absence (the He, ISD data) and presence (the N_2, ECR data) of collisional effects.

Equation (4) may be rewritten as

$$\lambda_m(\text{cm}) \cong 10^{-2}(\sqrt{\mu_i T_e}/B)\sin\psi, \tag{5}$$

where μ_i is the ion mass normalized to hydrogen, T_e is the electron temperature in eV, B is the magnetic field in Gauss,

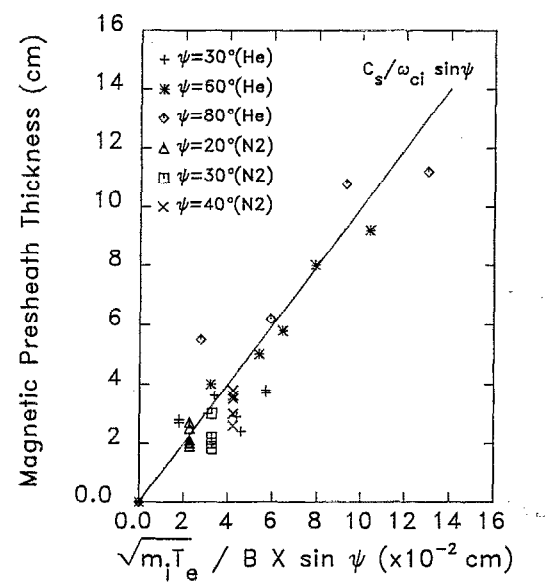

FIG. 8. The measured thicknesses of the magnetic presheaths in the absence of collisional effects (ISD, helium plasmas) and in the presence of collisional effects (ECR, nitrogen plasmas) versus $r_{cs}\sin\psi$, where the ion sound gyroradius $r_{cs}\equiv C_s/\omega_{ci}$. The ion sound velocity C_s is $\sqrt{T_e/m_i}$ (in these experiments $T_e \gg T_i$), and ω_{ci} is the ion gyrofrequency. The solid line is $\lambda_m = r_{cs}\sin\psi$ and, hence, these data show that $\lambda_m \cong r_{cs}\sin\psi$ regardless of the absence or presence of collisional effects.

and it has been assumed that $T_e \gg T_i$, so that C_s is $\sqrt{T_e/m_i}$. The assumption $T_e \gg T_i$ is valid for the data presented here.

Equation (5) suggests that λ_m is dependent on μ_i, T_e, B, and Ψ, and indeed the data show this to be true. The μ_i differed in the ISD (helium $\mu_i=4$) and ECR (nitrogen $\mu_i=28$) experiments. The T_e also differed between the ISD (~7 eV) and ECR (3–5 eV, depending on the neutral pressure) experiments. Magnetic field B was varied in the ISD experiments (from 40 to 170 G), and was approximately 175 G in the ECR experiments. The angle Ψ was varied from 30° to 80° in the ISD experiments and from 0° to 40° in the ECR experiments. Even though the λ_m's from ECR experiments are slightly shorter than those from ISD experiments, the data shown in Fig. 8 verify the dependence of λ_m on μ_i, T_e, B, and Ψ according to Eq. (5).

C. Our experimental magnetic presheath thickness results and Chodura's theory

As was just discussed in the previous section, our experimental presheath thickness data show $\lambda_m \cong r_{cs} \sin\psi$ (see Fig. 8); and also the same result was obtained from PDP1 numerical simulation (see the Appendix). On the other hand, Chodura's theory[16] predicts $\lambda_m = \sqrt{6} r_{cs} \sin\psi$ [see Eq. (3)]. Hence, qualitatively, our data and Chodura's theory are in agreement. Quantitatively, however, there is a $\sqrt{6}$ discrepancy. This discrepancy may be, in part, due to the assumptions by Chodura that ions enter (at their thermal velocity) a presheath (of approximate length $L/2$ and potential drop $T_e/2$), and are accelerated as they follow field lines in that presheath so that they enter the magnetic presheath with a velocity C_s along the field lines (see the additional "presheath region" in Fig. 2). With the exception of data at low B and high Ψ, our measurements do not show a quasineutral presheath of approximate length $L/2$ and potential drop $T_e/2$. Further, even if there was such a presheath, Chodura's assumption that ions in that presheath follow field lines is not consistent with our device parameters. For example, in ISD, the $\mathbf{E}\times\mathbf{B}$ drift velocity $V_{E\times B}=E/B \approx (T_e/LB) \approx 7$ V/(0.36 m)(0.01 T)$\approx 2\times 10^3$ m/s, which is approximately a tenth of the sound speed. When the magnetic presheath becomes thicker, the additional presheath should be thinner, the electric field in the presheath is stronger, and $V_{E\times B}$ larger. Note that this drift velocity is normal to the E and B field directions. In the (small chamber) ISD experiment, therefore, the ions would not travel strictly along field lines in the region of Chodura's presheath near the bulk plasma.

One should also note that both models, ours (Fig. 1, which was based on experiments) that has only a magnetic presheath, and Chodura's (Fig. 2) that has both a presheath and a magnetic presheath, have difficulties at certain extreme limits. Our model has difficulties at low Ψ. As Ψ approaches zero, our magnetic presheath thickness $\lambda_m = r_{cs} \sin\psi$ approaches zero. However, we expect that as Ψ approaches zero, the presheath becomes unmagnetized and its length becomes $L/2$. Chodura's model has difficulties at low B, for which $V_{E\times B}=E/B$ becomes large and for which r_{cs} becomes larger. As $r_{cs} \to L/2$, there is no longer room for a "presheath" of length $L/2$.

D. Potential drop in the magnetic presheath

In our model, the particle motion is influenced by both the magnetic and electric fields. The magnetic field is introduced externally, while the electric field is generated by the plasma, in order that the Bohm criterion at the sheath boundary is satisfied. Through calculations of single-particle motion from the equation of the ion motion and ion energy conservation, we can obtain the potential drop in the magnetic presheath with the following assumptions: uniform electric field directed toward the wall normally and magnetic fields at an angle Ψ with respect to the electric field in the magnetic presheath; ions enter the magnetic presheath with thermal velocity ($\cong 0$ because $T_e \gg T_i$); the magnetic presheath thickness is the measured value $\lambda_m \cong r_{cs} \sin\psi$; and, finally, ions enter the sheath with C_s normal to the sheath boundary.

The equation of motion for ions is

$$m \frac{d\mathbf{v}}{dt} = q(\mathbf{E} + \mathbf{v}\times\mathbf{B}), \tag{6}$$

where m is ion mass. Letting $\mathbf{E}=E\hat{x}$ and $\mathbf{B}=B_x\hat{x}-B_z\hat{z}$, where $\hat{x}$ is in the direction normal to the wall (as shown in Fig. 1), and assuming that both fields do not vary with y direction, the ion velocity components, $v_x(t)$, $v_y(t)$, and $v_z(t)$, from Eq. (6), are

$$v_x(t) = \epsilon_x[t-(t-\sin(\omega_{ci}t)/\omega_{ci})\sin^2\Psi] - v_{y0}\sin\Psi\sin(\omega_{ci}t) + v_{x0}, \tag{7a}$$

$$v_y(t) = \epsilon_x[1-\cos(\omega_{ci}t)]\sin\Psi/\omega_{ci} + v_{y0}\cos(\omega_{ci}t), \tag{7b}$$

$$v_z(t) = -\epsilon_x[t-\sin(\omega_{ci}t)/\omega_{ci}]\sin\Psi\cdot\cos\Psi + v_{y0}\cos\Psi\sin(\omega_{ci}t) + v_{z0}, \tag{7c}$$

where $\epsilon_x = qE/m_i$ and $\omega_{ci} = qB/m_i$. Using this model, the ion motion can be described with the aid of conservation of energy. If the total ion energy in the magnetic presheath is conserved, then

$$e\Phi_m = \tfrac{1}{2}m(v_x^2+v_y^2+v_z^2), \tag{8}$$

where Φ_m is the potential drop in the magnetic presheath and m is the ion mass. The electric field can be calculated by dividing Eq. (8) with the magnetic presheath thickness,

$$E = \frac{\Phi_m}{\lambda_m} = \frac{1}{2}m\frac{(v_x^2+v_y^2+v_z^2)}{\lambda_m}. \tag{9}$$

The measured λ_m was found to be well described by

$$\lambda_m = r_{cs}\sin\psi. \tag{10}$$

Ion enters the sheath with ion sound speed and no initial velocity, so

$$v_x(t_s) = C_s, \tag{11}$$

where t_s is the time at which it reaches to the sheath. The time t_s and the electric field can be obtained simultaneously

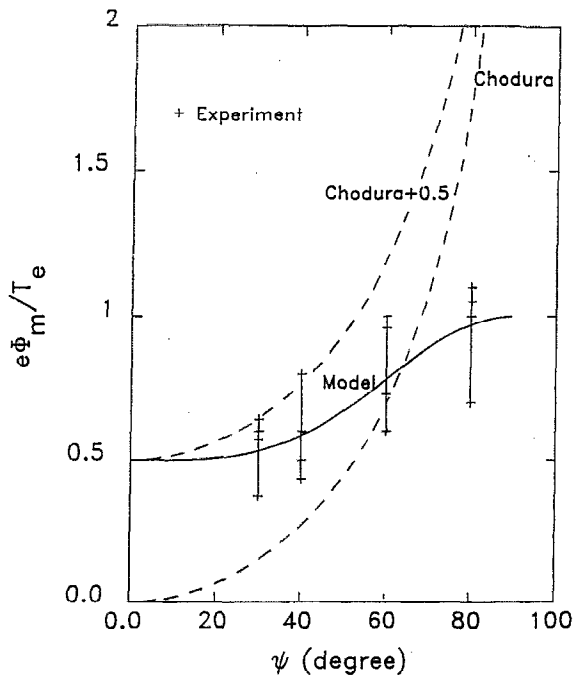

FIG. 9. The normalized (by 7 eV, the typical electron temperature in ISD) potential variations in the magnetic presheath versus the magnetic field angle, with the error bars indicating the spread in the data at the same magnetic field angle. The dotted lines indicate Chodura's theoretical result [see Eq. (3)] and the solid line is the simulated result from Eq. (12).

by integrating Eq. (7) and Eq. (8) using the boundary conditions in Eqs. (10) and (11). The result for the Φ_m is

$$\Phi_m \approx \frac{1}{2e}(1+\sin^4\psi)T_e. \tag{12}$$

Note that Φ_m depends only on Ψ and T_e.

Figure 9 shows the measured normalized potential drop $e\Phi_m/T_e$ (where $T_e \cong 7$ eV) across collisionless magnetic presheaths versus Ψ for conditions similar to those in which the data shown in Figs. 5–7 were obtained. The predictions of Chodura's theory [Eqs. (2)–(3)], as well as the numerical results from a single-particle model of ours are also shown for comparison.

Inspection of Fig. 9 shows that the solid line that represents our simulation results carried out without Chodura's additional presheath assumption is in fairly good agreement with the experimental results, while both the lower dotted line that represents Chodura's prediction, $\Delta\Phi_m^T = (T_e/e)\ln(\cos\psi)$ and the upper dotted line represents Chodura's prediction plus $0.5T_e$ (to take into account the additional presheath potential drop) do not agree with the experimental results. This discrepancy between the measured potential drop in the magnetic presheath and Chodura's theory may be in part due to those assumptions made by Chodura that are not applicable to our plasma. Also note that the good agreement between our simulation results and data support the validity of the assumptions that the Bohm criterion is satisfied at the sheath edge, and that $\lambda_m \cong r_{cs}\sin\psi$.

V. COLLISIONAL-MAGNETIC PRESHEATH EXPERIMENTAL RESULTS AND DISCUSSION

A. Collisional-magnetic presheath measurements in ECR etcher

In previous sections, data showing magnetic presheaths in the absence of collisions were presented. Data showing collisional presheaths in the absence of magnetic effects were presented by Meyer *et al.*[2] They found quasineutral collisional presheaths, which the plasma creates to satisfy the Bohm sheath criterion, and found that the thicknesses of these collisional presheaths are proportional to the mean-free path. In this section, data showing collisional-magnetic presheaths (i.e., presheaths in the presence of both collisional and magnetic field effects) are presented. The data show that collisional-magnetic presheaths consist of two distinctive regions: one collisional and the other magnetic in character. The data show that these two regions are independent of one another and that the collisional region displays the same qualitative and quantitative behaviors as collisional (in the absence of magnetic effects) presheaths, while the magnetic region has the same qualitative and quantitative behaviors as magnetic (in the absence of collisional effects) presheaths. The collisional region of the collisional-magnetic presheaths will, therefore, be henceforth referred to as the collisional presheath part of the collisional-magnetic presheath, while the magnetic region will be referred to as the magnetic presheath part of the collisional-magnetic presheath.

Figure 10(a) shows plasma equipotential contours in front of a plate in an ECR nitrogen plasma with 800 W, 2 mTorr, and $\Psi = 20°$. The magnetic fields corresponding to Figs. 10–12 are approximately axial. Fig. 10(b), a graph of the corresponding Φ_p versus axial position for a certain radial position ($r = -1$ cm), illustrates the method by which the locations of the open circles and squares of Figs. 10–12 are chosen. Each circle denotes the position of the first discontinuity in the slope of the measured plasma potential versus the axial position (at a given radial position) that is observed as the probe moves axially away from the plate. The squares denote the second discontinuity.

In Figs. 10–12, the regions between the plate and the open circles are the sheath and the collisional presheath parts of the collisional-magnetic presheath. In the ECR plasmas, sheaths are of too small a dimension (approximately 0.1 mm) to be measured by our probes, and will henceforth be neglected. Hence, the regions and distances between the plate and open circles will hereafter be considered and referred to as the collisional presheath part of and the collisional presheath thickness λ_c of the collisional-magnetic presheath, respectively.

Comparisons of Fig. 10(a) with Figs. 11(a) and 11(b) show that λ_c varies with neutral pressure and is independent of Ψ, respectively. Table II(a) summarizes the results of a quantitative analysis of the data, which found λ_c proportional to the ion–neutral collision mean-free path λ_n, and in good agreement with (although slightly less than) the collisional presheath thickness found by Meyer *et al.*[2] in the absence ($\Psi = 0°$) of magnetic field effects (that experiment was also carried out in an ECR device, in which there was a

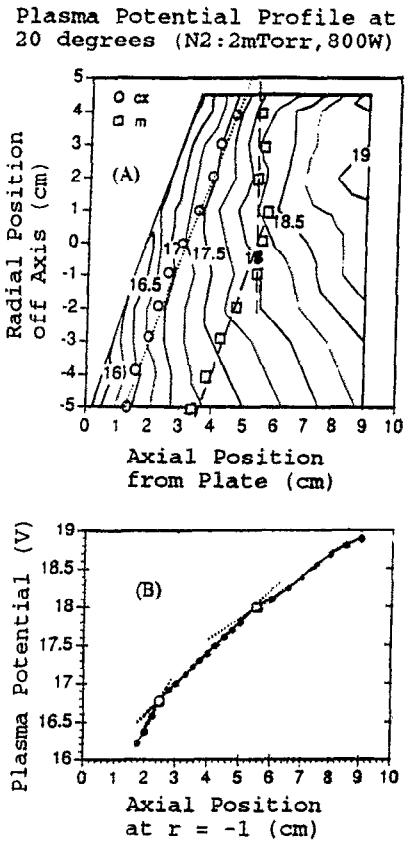

FIG. 10. (A) Equipotential contours in an ECR nitrogen plasma with 800 W, 2 mTorr, and $\Psi=20°$. (B) The corresponding plasma potential (V) versus axial position (cm) for a radial position of $r=-1$ cm. Squares represent the magnetic presheath/bulk plasma boundary and open circles represent the collisional presheath/magnetic presheath boundary. The magnetic field is approximately axial.

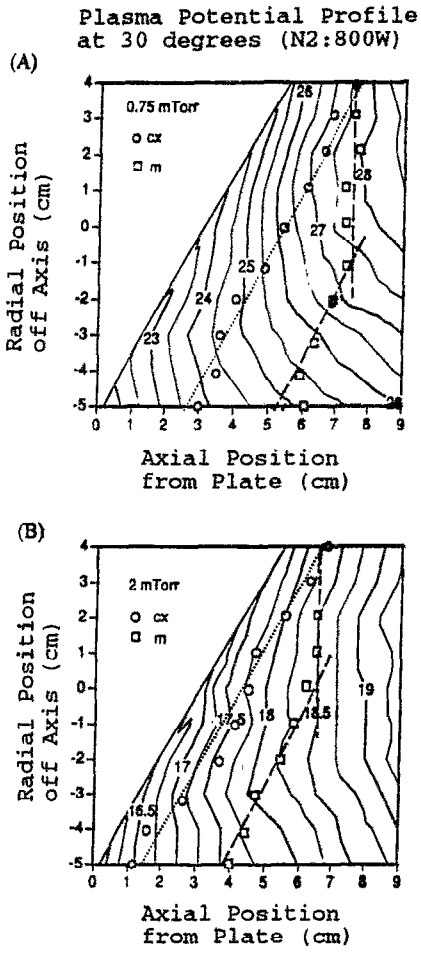

FIG. 11. Equipotential contours for different pressures: (A) 0.75 mTorr and (B) 2 mTorr in ECR nitrogen plasmas with 800 W and $\Psi=30°$. Squares represent the magnetic presheath/bulk plasma boundary and circles represent the collisional presheath/magnetic presheath boundary.

nonzero magnetic field. However, in that experiment, the nondivergent magnetic field along the axis, where the data were taken, was perpendicular to the plate, i.e., $\Psi=0°$; and, hence, no magnetic effects were expected nor were any observed). Hence, the collisional presheath displays the same behavior, regardless of the absence or presence of magnetic field effects.

In Figs. 10–12, some squares run parallel to the plate and open circles, while other squares run vertically, i.e., perpendicular to B and radially in the device. The regions between the open circles and the vertically running squares are the magnetic presheath regions that are affected by finite boundaries (see Sec. V C). The regions between the open circles and the squares running parallel to them are the regions that are not affected by finite boundaries. When we refer to the thicknesses λ_m of the magnetic region of the collisional-magnetic presheath, we are referring to the thicknesses of the later (not affected by finite boundaries) regions, unless otherwise noted.

A comparison of Figs. 10(a), 11(b), and 12(b) shows that λ_m (the distance between the open circles and the squares that fall in a line parallel to the circles) increases with increasing Ψ. As was mentioned previously, λ_m is well described by Eq. (4). Table II(b) (also N_2 data in Fig. 8) summarizes the results of a quantitative comparison, which found λ_m in the presence of collisions to be only slightly less than in the absence of collisions. Hence, similar to the lack of magnetic field effects on collisional presheaths, magnetic presheaths display approximately the same behavior, regardless of the absence or presence of collisional effects.

There is a variation in λ_m of with neutral pressure. The variation is most apparent in a comparison of Figs. 12(a) (which shows no open squares because they are outside the scanning range of the probe) and 12(b), although it can also be seen in a comparison of Figs. 11(a) and 11(b). The reader, however, should not assume that this data suggests λ_m is affected by collisional effects. Rather, T_e varies with neutral pressure and λ_m is dependent on T_e (specifically, $\lambda_m \propto r_{cs} \propto C_s \propto \sqrt{T_e}$). Indeed, the data at all pressures show $\lambda_m \cong r_{cs} \sin \psi$.

A comparison of Figs. 10(a), 11(b), and 12(b) shows that even when Ψ is varied the bulk plasma potential at $z=8$ cm and $r=2$ cm is constant, approximately 19 V, because all the boundaries are grounded and the operating conditions (flow rate, neutral pressure, and power) are the same. However,

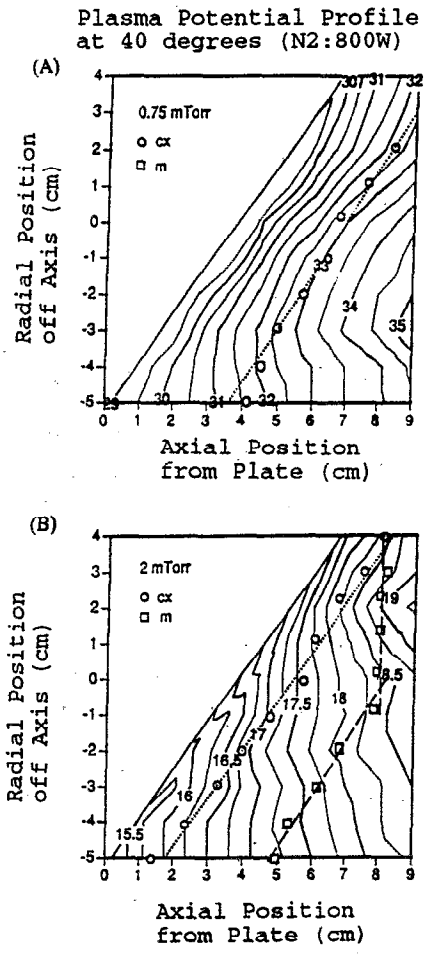

FIG. 12. Equipotential contours for different pressures: (A) 0.75 mTorr and (B) 2 mTorr in ECR nitrogen plasmas with 800 W and $\Psi=40°$. Squares represent the magnetic presheath/bulk plasma boundary and circles represent the collisional presheath/magnetic presheath boundary.

TABLE II. (a). Collisional presheath thicknesses λ_c in the absence ($\Psi=0°$, the * values are from Ref. 10) and presence ($\Psi\neq0°$) of magnetic field effects. Here P_0 is the neutral pressure. (b) Magnetic presheath thicknesses λ_m in the absence and presence of collisional effects. Here Ψ is the angle between the magnetic field and the normal to the boundary. Here ** indicates the calculated values from Eq. (4) with $T_e=3$ eV and $B=175$ G.

(a)	P_0 (mTorr)	$\Psi(°)$	λ_c (cm)
	2	$\neq0$	$\cong$2.0
	2	$=0$	$\cong$1.3*
	0.75	$\neq0$	2.2–2.5
	0.75	$=0$	$\cong$3.0*
(b)	$\Psi(°)$	Collisional effects	λ_m (cm)
	40	Present	$\cong$2.4
	40	Absent	3.4**
	30	Present	2.2–2.5
	30	Absent	2.6–2.9
	20	Present	$\cong$2.0
	20	Absent	1.8**

TABLE III. (a). The normalized potential difference $e\Phi_c/T_e$ across collisional presheaths in the absence ($\Psi=0°$, the * values are from Ref. 10) and presence ($\Psi\neq0°$) of magnetic field effects. Here P_0 is the neutral pressure and T_e is the electron temperature. (b) The normalized potential difference $e\Phi_m/T_e$ across magnetic presheaths in the absence and presence of collisional effects. Ψ is the angle between the magnetic field and the normal to the boundary and T_e is the electron temperature. Here ** indicates the calculated values for Eq. (12).

(a)	P_0 (mTorr)	Magnetic effects	$e\Phi_c/T_e$
	2	$\Psi\neq0°$	0.17–0.33
	2	$\Psi=0°$	0.47*
	0.75	$\Psi\neq0°$	0.38–0.59
	0.75	$\Psi=0°$	0.48*
(b)	$\Psi(°)$	Collisional effects	$e\Phi_m/T_e$
	40	Present	0.33
	40	Absent	0.59**
	30	Present	0.27
	30	Absent	0.4–0.6
	20	Present	0.23
	20	Absent	0.51**

comparison of Figs. 11(a) and 12(a) shows that the location of the peak plasma potential region shifts from $r=3$ cm in Fig. 11(a) to $r=-3$ cm in Fig. 12(a). As shown in Fig. 12(a), the magnetic presheath region is extended into the source plasma, i.e., the source plasma is perturbed by the tilted boundary.

B. Potential variation in the collisional-magnetic presheath

A comparison of the potential drops normalized to T_e across the collisional presheaths in the presence and absence of magnetic effects is shown in Table III(a). The typical T_e's at different Ψ are chosen at different axial positions because the location of the collisional presheath moves toward the source chamber with Ψ, as mentioned previously. Note that the normalized potential drops across collisional presheaths increase with decreasing pressure when magnetic field effects are present and do not depend on pressure when magnetic effects are absent. It is observed that these potential drops are insensitive to the angle variation.

For comparison, the normalized potential drops across magnetic presheaths in the presence and absence of collisional effects are presented in Table III(b). Note that the normalized potential drops across magnetic presheaths increase with increasing Ψ, but that the increases are smaller when collisional effects are absent.

An inspection of the values of Tables III(a) and III(b) shows the total normalized potential across the presheath $e\Phi_c/T_e+e\Phi_m/T_e$ is roughly constant, regardless of the presence or absence of collisional or magnetic effects [$e\Phi_m$ in the absence of collisional effects (for which $e\Phi_c$ is set to zero) and $e\Phi_c$ in the absence of magnetic field effects (for which $e\Phi_m$ is set to zero) are roughly equal]. The total normalized potential drop in the collisional-magnetic presheath is slightly greater than the potential drops across collisional and magnetic presheaths, in the absence of magnetic and

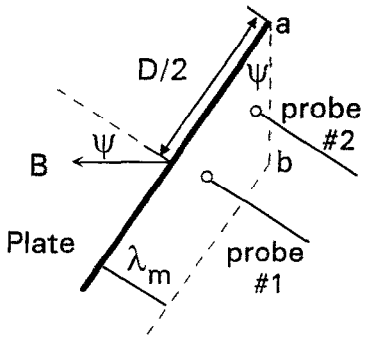

FIG. 13. The qualitative illustration of the finite boundary effect.

collisional effects, respectively. This suggests that ions in collisional-magnetized presheaths need slightly more energy to get the Bohm speed normal to the sheath.

As mentioned previously, the bulk plasma potential Φ_p was independent of Ψ. Because the boundary was grounded, $\Phi_p=\Phi_s+\Phi_{cm}$, where Φ_{cm} is the potential variation in the collisional-magnetic presheath. Hence, Φ_s in collisional, magnetized plasmas varies when Φ_{cm} varies. When Φ_{cm} increases slightly Φ_s decreases slightly.

C. The finite boundary effect

As noted in Sec. V A, in Figs. 10–12, some open squares run perpendicular to B, i.e., vertically in the Figures (the magnetic fields corresponding to Figs. 10–12 are approximately axial), while others fall in a line parallel to the plate and open circles. The plate is 11 cm in diameter and pivots about a point at approximately $(r,z)=(-5$ cm, $+0.2$ cm), where r and z are the radial and axial coordinates, respectively. For $\Psi=20°$ [Fig. 10(a)], 30° [Figs. 11(a) and 11(b)], and 40° [Fig. 12(b); we will not consider Fig. 12(a) in this discussion because the open squares fall out of the scanning range of the probe], the intersections of the open squares and circles occur at approximately $r=5.0$ cm (for $\Psi=20°$), 4.5–4.0 cm (for $\Psi=30°$), and 3.5 cm (for $\Psi=40°$), respectively.

Let us suppose that in the absence of collisions, the boundaries between magnetic presheaths and bulk plasmas are similar to those shown in Figs. 10–12. Such a situation is depicted in Fig. 13. As drawn in Fig. 13, probe #2 is a bad measure of λ_m; probe #2 underestimates λ_m. Should the field decrease so that λ_m increases, probe #2 would measure no change.

Our probe scans along a line that passes through the center of the plate, as does probe #1 of Fig. 13. As shown, probe #1 is an accurate measure of λ_m. However, for smaller B, probe #1 encounters the same problem (the same finite boundary effect) as probe #2. In particular, when the line segment ab becomes greater than the square root of $(D/2)^2+(\lambda_m)^2$, probe #1 will pass through the line segment ab and the λ_m it measures will be constant for decreasing B (as is the case for the $B\leqslant 85$ G data shown in Fig. 7).

Note that the line segment ab is equal to $\lambda_m \sin\Psi$. Since it was experimentally determined that $\lambda_m \cong r_{cs} \sin\psi$, our probe will not measure a change λ_m whenever B is small enough to satisfy

$$\left(\frac{C_s}{\omega_{ci}}\right)^2 \geqslant \left(\frac{D}{2}\right)^2 + \left[\left(\frac{C_s}{\omega_{ci}}\right)\sin\psi\right]^2, \tag{13}$$

which can be rewritten as

$$C_s/\omega_{ci} \geqslant D/(2\cos\psi)$$

or

$$B(\mathrm{G}) \leqslant 2\times 10^3 \cos\Psi/D(\mathrm{cm}). \tag{14}$$

Hence, for the conditions under which the data of Fig. 7 was taken ($\Psi=30°$, $D=15$ cm), one would expect, because of the finite boundary effect, that the probe would measure a constant magnetic presheath thickness for $B\leqslant 115$ G. Note that this expectation is consistent with the observed data. Hence, the finite boundary effect can explain the data shown in Fig. 7.

VI. CONCLUSION

In collisional, magnetized plasmas, it is observed that the presheath has a double structure composed of a collisional presheath and a magnetic presheath. These magnetic (collisional) presheaths have thicknesses that are found to be insensitive to collisional (magnetic) effects, respectively. Magnetic presheath thickness λ_m is found to be approximately $C_s/\omega_{ci} \sin\psi$ and vary with ion mass, electron temperature, magnetic field, and angle Ψ between the magnetic field and the boundary. The finite boundary effect can distinguish magnetic presheaths from collisional presheaths. Collisional presheath thicknesses vary with the ion–neutral collision mean-free path.

Collisional-magnetic presheaths are found to have an approximately $0.5T_e/e$ (roughly satisfying the Bohm criterion) potential difference across them for $\Psi\leqslant 40°$.

ACKNOWLEDGMENTS

The authors wish to express their many thanks to J. Meyer for his helpful suggestions regarding collisional presheaths.

The research is supported by National Science Foundation Grants No. ATM-9017451 and No. ECD-8721545 for the Engineering Research Center for Plasma-Aided Manufacturing.

APPENDIX: PDP1 SIMULATION

The PDP1 simulation[35] is one of the techniques that was employed to understand the physics of magnetic presheaths. The scheme of PDP1 is described detail in Ref. 34. Figure 14 shows the simulation results taken with the following conditions. The simulation region is rectangular in shape, 2 cm in length, and 1 cm^2 in area. The half-Maxwellian particles have an electron temperature (0.23 eV) ten times greater than the ion temperature (0.023 eV). The particles are injected from the midpoint of the left boundary. The time step (δt) is chosen as 4.9×10^{-10} s by consideration of the condition

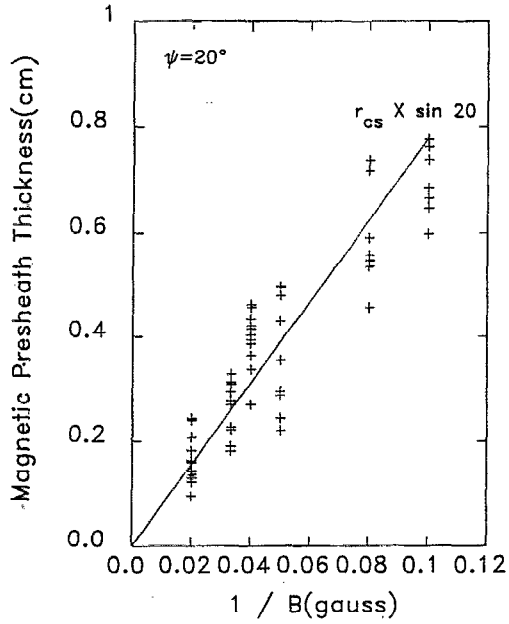

FIG. 14. The measured thickness of magnetic presheaths from PDP1 numerical simulation[35] at $\Psi=20°$ vs $1/B$.

$\omega \cdot \delta t \leqslant 0.2$, where ω was chosen as the highest frequency (electron gyrofrequency is ~10 GHz) used in this simulation. The injection flux was fixed and the ion–electron mass ratio was 400. Collision and ionization were not considered. The angle Ψ between the magnetic field and the plate normal was fixed to 20°. The magnetic field was varied from 10 G (the corresponding magnetic presheath thickness at $\Psi=20°$ is approximately 0.79 cm) to 50 G (approximately 0.16 cm). The ion and electron densities at the center of the system were $2–4\times10^7$ cm^{-3}, and Debye lengths were on the order of 0.1 cm. The potential, electric field, velocity distribution, ion density, and electron density profiles were shown as snapshots at each time interval. The simulation was run until the particle number in the system became a constant, that is, when the number of incoming particles was equal to the number leaving the system.

The simulation results also show a magnetic presheath structure. The sheath and presheath boundaries are obtained by choosing the positions where the slopes change sharply in the following profiles: plasma potential, electric field, ion density, electron density, and velocity distribution. These results are shown in Fig. 14. The thickness of the sheath is approximately 2.5 Debye lengths. Figure 14 shows that the measured thickness of the magnetic presheaths are proportional to $\sin \Psi/B$.

[1] I. Langmuir and H. M. Mott-Smith, Gen. Electron. Rev. **27**, 499 (1924).
[2] J. A. Meyer, G.-H. Kim, M. J. Goechkner, and H. Hershkowitz, Plasma Sources Sci. Technol. **1**, 147 (1992).
[3] G. F. Matthews, S. J. Fielding, G. M. McCracken, C. S. Picher, P. C. Stangeby, and M. Ulrickson, Plasma Phys. Controlled Fusion **32**, 1301 (1990).
[4] T. Intrator, J. Menard, and N. Hershkowitz, Phys. Fluids B **5**, 806 (1992).
[5] J. R. Sanmartin, Phys. Fluids **13**, 103 (1970).
[6] E. R. Harrison and W. B. Thompson, Proc. Phys. Soc. **74**, 145 (1959).
[7] P. C. Stangeby and J. E. Allen, J. Phys. A Gen. Phys. **3**, 304 (1970).
[8] J. E. Allen, in *Plasma Physics*, edited by B. E. Keen (Institute of Physics, Bristol, 1973), Chap. 5.
[9] J. E. Allen, J. Phys. D: Appl. Phys. **9**, 2331 (1976).
[10] D. Bohm, in *The Characteristics of Electrical Discharges in Magnetic Fields*, edited by A. Guthrie and R. K. Wakering (McGraw-Hill, New York, 1949), Chap. 3.
[11] G. Emmert, R. M. Wieland, T. Mense, and J. N. Davidson, Phys. Fluids **23**, 803 (1980).
[12] S. Meassick, M. H. Cho, and N. Hershkowitz, IEEE Trans. Plasma Sci. **PS-13**, 115 (1985).
[13] P. C. Stangeby, Phys. Fluids **27**, 682 (1984).
[14] K-U. Riemann, J. Phys. D Appl. Phys. **24**, 493 (1991).
[15] G. E. Main, Phys. Fluids **30**, 1800 (1987).
[16] R. Chodura, Phys. Fluids **25**, 1628 (1982).
[17] R. Chodura, in *Physics of Plasma–Wall Interactions in Controlled Fusion*, edited by D. E. Post and R. Behrisch (Plenum, New York, 1986), pp. 99–134.
[18] U. Daybelge and B. Bein, Phys. Fluids **24**, 1190 (1981).
[19] A. B. DeWald, A. W. Bailey, and J. N. Brooks, Phys. Fluids **30**, 267 (1987).
[20] K.-U. Riemann, Contrib. Plasma Phys. **32**, 231 (1992).
[21] J. Behnel, in *12th EPS Conference on Controlled Fusion and Plasma Physics* (European Physical Society, Geneva, 1985) Vol. 9F, Part II, p. 468.
[22] K. Theihaber and C. K. Birdsall, Phys. Fluids B **1**, 2244, 2260 (1989).
[23] R. Chodura, Contrib. Plasma Phys. **28**, 303 (1988).
[24] G. Fiksel, M. Kishinevsky, and N. Hershkowitz, Phys. Fluids B **3**, 834 (1991).
[25] S. C. Brown, *Basic Data of Plasma Physics 1966*, 2nd ed. (MIT Press, Cambridge, MA, 1976).
[26] G.-H. Kim, Ph.D. thesis, University of Wisconsin—Madison, 1993.
[27] R. G. Little and J. F. Waymouth, Phys. Fluids **9**, 801 (1966).
[28] M. E. Koepke and W. E. Amatucci, IEEE Trans. Plasma Sci. **PS-20**, 631 (1992).
[29] P. Coakley, Ph.D. thesis, University of Iowa, 1980.
[30] R. F. Kemp and J. M. Sellen, Jr., Rev. Sci. Instrum. **37**, 455 (1966).
[31] D. Diebold, N. Hershkowitz, A. D. Bailey, III, M. H. Cho, and T. Intrator, Rev. Sci. Instrum. **59**, 270 (1988).
[32] J. R. Smith, N. Hershkowitz, and P. Coakley, Rev. Sci. Instrum. **50**, 210 (1979).
[33] H. Fuzita, S. Yagura, and E. Yamata, J. Phys. Soc. Jpn. **50**, 3759 (1981).
[34] M.-H. Cho, Ph.D. thesis, University of Wisconsin—Madison, 1988.
[35] C. K. Birdsall and A. B. Langdon, *Plasma Physics Via Computer Simulation* (McGraw-Hill, New York, 1985).